PRELIMINARY RESULTS IN INVESTIGATION OF DIFFRACTIVE HIGH-EFFICIENCY OBJECTIVES

V.P. Korolkov[1], C. Pruss[2], S. Reichelt[2], H.J. Tiziani[2],
[1]Institute of Automation and Electrometry SB RAS, Novosibirsk, 630090, Russia
[2]Institut für Technische Optik, Universität Stuttgart, Germany

It has been shown that high-efficiency diffractive objectives are an alternative to their refractive counterparts for applications requiring high precision transformation of monochromatic light (for example in interferometers). A 80 mm diameter prototype (N.A. - 0.158; design wavelength - 632.8 nm) has been fabricated by direct laser writing on photoresist. It was manufactured on a polar coordinate laser writing system CLWS-300 that is able to write high precision DOEs up to a diameter of 300 mm. The blazed diffractive structures were written directly into a photoresist layer that was spinned on a high-precision substrate. The fabricated objective has a rms wavefront error of less than λ/20 in single pass. The residual errors are predictable using manufacturing data that is recorded during the writing process for each element. This permits to provide each element with calibration data. Measurements of the fabricated DOEs show excellent agreement between the predicted and measured wavefront quality.

Introduction

Objectives for collimation and adaptation of wavefronts are important part of many optical measurement devices. When measurement resolution should be less than wavelength the proper fabrication errors of an objective becomes rather essential. However, refractive objectives have a limited optical quality that is usually not better than λ/2 for large diameters. The relatively low quality of large diameter objectives requires a very careful calibration of the optical setup to eliminate the influence of fabrication errors of the objective.

A way to increase the accuracy of objectives while dramatically reducing weight and complexity and still maintaining a reasonable price is diffractive optics. Diffractive optics have been used for years in optical testing of aspheric surfaces and are on their way to becoming an established technique [1, 2, 3, 4]. In this application, the high accuracy of the generated wavefronts is essential and has been analyzed and demonstrated in detail. Problems due to chromatic aberrations introduced by the strong dispersion inherent to diffractive optical elements (DOE) do not occur when monochromatic light is used.

Until now mainly *binary* diffractive optics were used for optical testing because of the relative simplicity of their fabrication. The drawback of these structures is the relatively low diffraction efficiency of about 40% for binary phase structures. For objectives, a higher efficiency is required. The development of fabrication technologies in diffractive optics permits to manufacture high-efficiency, large aperture DOEs. This allows the realization of diffractive objectives, either as a purely diffractive element or as a hybrid combination of refractive and diffractive surfaces. In the paper we present our results on manufacturing and testing a high-efficiency DOE being a base element for future design of high-accuracy objectives.

Different techniques have been mentioned in literature to fabricate high-efficiency DOEs. A common approach is the multi-mask technique that produces elements with 2^N phase levels with N binary masks. The many fabrication steps required in this technique are time consuming and sensitive to alignment errors. For the manufacturing of high-precision objectives, we have chosen to use a single-step, gray scale technique. Gray scale fabrication is a way to avoid many steps. In principle, there are two ways to produce many phase levels in one step. One way is to generate a gray scale mask that is used in a second step to illuminate a photoresist layer at contact printing. This gray scale mask can be made the base of material with variable transmission like HEBS-glass or LDW-glass [5]. The second approach is to write the structure directly into photoresist. The approach with gray scale masks has some disadvantages for the fabrication of large diameter high precision diffractive objectives:

- additional fabrication step (contact printing) brings in additional phase errors;
- fabrication of large GSM is currently a very expensive process.

Thus, the second approach with direct laser writing on photoresist is most suitable for fabrication of individual, high-precision diffractive objectives. The results in this paper are based on elements written directly into photoresist.

1. Fabrication method

In the present work, we report on results of our investigations on a diffractive objective written by means of the circular laser writing system CLWS-300 [1] specially modernized for writing of multi-level DOEs. It is a highly universal tool for the fabrication of diffractive optical elements such as computer-generated holograms, zone plates, gratings, optical scales, etc. The substrate for patterning is fixed on the faceplate of a precision air-bearing spindle. A high accuracy rotary encoder is mounted on the spindle axis. The rotary optical encoder delivers the signal for the stabilization of the rotation speed and for synchronizing the laser beam power modulation with the turning of substrate. An argon ion

laser is mounted on the granite base with the vibration isolator supports. The laser radiation (50-100 mW at 457 nm wavelength) is modulated by two acousto-optic modulators. Two modulators were needed to get high contrast of beam power modulation, which is required for compensating a change of linear scanning speed (and, correspondingly, exposure time) with radial coordinate. However even two modulators are not enough to compensate changing a linear scanning speed in range 10^{-2}–10^{3} mm/s and supply accurate analog modulation. Using pulse writing mode near rotation center (0-3 mm radial coordinate range) circumvented this problem. This mode consists of exposing circular tracks by a series of short pulses of laser radiation with constant pulse duration (0.3-0.6 μs) and variable period. The period τ of pulses at writing is chosen based on a condition of constant overlapping size of the adjacent light spots:

$$\tau = \delta / 2\pi r \nu ,$$

where r - the radius of a written ring track, ν - rotation speed of substrate, δ - constant linear distance between points of switching on the adjacent pulses. Previous test writing on photoresist is used to match exposure doses at the boundary between pulse and continuous modulation modes. Modulated beam enters in the focusing objective through the optical system mounted on a mobile precision air-bearing linear stage. The linear stage is controlled interferometrically and allows a positioning of the writing head with an accuracy of ±30 nm. The focusing objective forms a light spot on the substrate surface with a diameter of about 1 μm. An autofocus subsystem maintains a constant spot size. For circular symmetric elements the system's symmetry (polar coordinate system) is especially advantageous. The substrate rotates at a constant rotation speed, which can be set in range of 200-600 rpm. The exposed rings are spaced evenly with a configurable radial increment between adjacent tracks.

In our experiments we used the photoresist Shipley S1828 and metal ion bearing (MIB) developers, which are most suitable for analog photoresist processing. To work in the practically linear part of the characteristic curve of the photoresist we used UV preexposing. A mask aligner provides the necessary uniform intensity distribution. The preexposure with energy dose E_{pre} also permits to reduce the influence of laser beam power fluctuations onto the relief depth. The coefficient of reduction can be estimated by the following equation for the total exposure dose:

$$\begin{aligned} E_{total} &= E_{pre} + E_{las} \cdot (1 + \Delta E_{las} / E_{las}) = \\ &= (E_{pre} + E_{las}) \cdot \left[1 + \frac{\Delta E_{las}}{E_{las}} \cdot \frac{E_{las}}{(E_{las} + E_{pre})} \right], \end{aligned} \quad (1)$$

where E_{las} is averaging energy dose from laser exposure, ΔE_{las} is the fluctuation of energy dose from laser exposure. Therefore the coefficient of reduction K_f of laser exposure fluctuations $\Delta E_{las}/E_{las}$ is defined as follows:

$$K_f = \frac{E_{las} + E_{pre}}{E_{las}} . \quad (2)$$

For a profile depth of 1 μm the value E_{las} is approximately equal to E_{pre}. Therefore K_f is equal to 2 for the maximum profile depth and increases with decreasing profile depth (with decreasing E_{las}).

1.1. Drift monitoring

A typical value for the writing time of large diffractive elements is several hours. During this time, the setup must be kept absolutely stable, since positioning errors directly influence on the generated wavefront. A distortion of the written structure caused by positioning errors results in wavefront aberrations that are proportional to the gradient of the recorded phase $\nabla\Phi(x,y)$:

$$W_{PD}(x,y) = -\zeta(x,y)\frac{m_D}{m_R}\frac{\lambda_0}{2\pi}\nabla\Phi(x,y) , \quad (3)$$

where $W_{PD}(x,y)$ is the resulting wavefront change, $\zeta(x,y)$ denotes the distortion vector of the DOE, m_D and m_R are the diffraction orders for design and reconstruction, respectively.

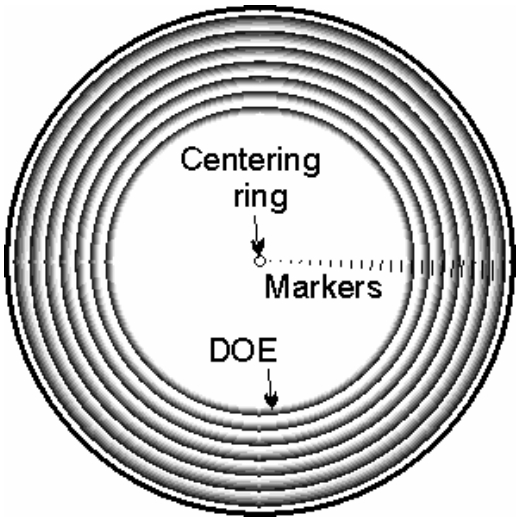

Fig. 1. Arrangement of high-reflective markers for recalibration of the radial coordinate during writing process

Since there is no way to avoid all mechanical drifts, the controlling software of the writing system monitors them and corrects current writing coordinate if it is necessary and wanted. Basis of the monitoring system is a net of markers that are formed on the substrate before direct laser writing on photoresist layer. These markers are segments of thin rings. Angular size of the segments is about 1-2°. The width in radial direction is about 1 micron. They are situated with period of 1-2 mm in whole radial range of fabricated DOE (Fig. 1). The markers are written on chromium film by thermochemical laser technology [6]. After laser writing on CLWS the substrate with Cr coating is developed in selective etchant removing unexposed film. As result, high reflecting markers are formed on the substrate, which is then coated by a photoresist. The substrate covered by photoresist is centered on the spindle of CLWS with an accuracy of ±0.25 micron by means of a large diameter centering chromium ring written together with the markers. One of the markers is used for search-

ing [10] the rotation center of the substrate. The controlling program defines its radial coordinates at the left and right of rotation center. The radial coordinate counter is set to zero at the middle point between these two values. Before the writing process on the photoresist layer the controlling program measures the positions of the markers by scanning a focused probe beam and measuring the power of reflected light. This measurement process is rapidly (< 1minute) made, and therefore no drift happens in the writing system. The obtained list of marker positions is used as reference. During the following writing process, when the radial coordinate of one of the markers is reached, the controlling program measures the position of this marker a second time. From the difference between the current and beforehand measured values the system calculates the effects of the mechanical drift and resets radial coordinate to value previously measured for this marker. As result, the small drift cumulative between two markers is eliminated. Described method of the drift monitoring has important advantages in comparing to known method [1] of rotation center search on the base of single central ring:

- less measurement time because of no need to move linear stage to rotation center;
- excellent compatibility with direct writing on curved surface because of no need to replace focusing objective in vertical direction for reading marker.

1.2. Selection and optimization of writing parameters

Controlling software of the writing system CLWS-300 writes rotationally symmetric multi-level DOEs using a circular scanning with constant radial increment. The beam power as function of radial coordinate and current phase level is calculated from a special table describing correspondence of the beam power and phase levels for several radial coordinate nodal points. The power for current radial coordinate is calculated between nodal points by linear approximation. The table is created from results of profile measurement on preliminary written test photoresist-coated sample. The profile measurement was made by microscope-interferometer MII-4 and atomic-force microscope. Exposure data in the table also depends on the rotation speed and radial increment.

The selection of the radial increment is very important step in the writing process. Preliminary modeling of the writing process was required in order to achieve higher diffraction efficiencies. The simulation yielded the following results concerning optimal radial increment. The overlap of neighboring exposure fields when scanning with a finite Gaussian beam is defined by the radial increment. The overlap and spot size define the obtained backward slope of the diffractive zones and the profile roughness. A larger track separation results in noticeable profile waves appearing on the photoresist surface. However smaller radial increment results in a less steep backward slope due to the integration over the tails of the overlapping exposure fields from many Gaussian spots. Fig. 2 shows the influence of the described factors on diffraction efficiency. We are referring to the diameter of the spot at the 1/e intensity level.

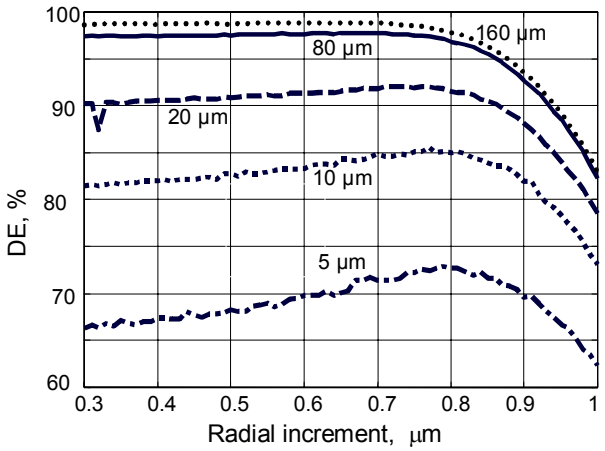

Fig. 2. Diffraction efficiency (DE) in the first order as function of the radial increment for Gaussian writing beam with spot size of 1 µm

Best efficiencies are obtained when the radial increment is about a factor of 0.7 smaller than the spot size. This value slightly depends somewhat on the structure size. For bigger track separations, noticeable profile waves start appearing on the photoresist surface. Smaller radial increments result in a less steep backward slope due to the overlap.

2. Experimental results

The diameter of the experimental objective was 80 mm. Its numerical aperture was 0.158. It was designed for λ=632.8 nm which leads to a minimal period of the diffractive zones of 4 µm for the first diffractive order. We studied wavefront aberrations and diffraction efficiency of manufactured elements.

2.1. Wavefront aberrations

With the help of the three position technique, the error of the interferometer inclusive the diffractive objective can be measured absolutely. Three separate interferometric measurements of a spherical test surface are required (test after Jensen) [1]. The first and the second measurements are made with the test surface positioned so that its center of curvature is at the focus of the positive diffractive lens (confocal position). After the first measurement, the test surface is turned by 180°. The third measurement is made with the vertex of the test surface at the focus of the positive zone lens, at the so-called cat's eye position. Fig. 3 shows the three required test setups.

With W_R as the aberration of the optics in the reference arm, W_O as the aberration of the optics in the test arm excluding that of the test surface and W_S as the aberration of the test surface, the three measurements can be written as:

$$\begin{aligned} W_1 &= W_S^0 + W_R^0 + W_O^0 \\ W_2 &= W_S^\pi + W_R^0 + W_O^0 \\ W_3 &= W_R^0 + \frac{1}{2}\left(W_O^0 + W_O^\pi\right), \end{aligned} \tag{4}$$

where the superscripts 0 and π indicates a rotation of the test piece by 0° or 180° respectively. This set of

equations can be solved for the aberrations of the interferometer $W_{INT} = W_O + W_R$, here represented by the expression $W_{PLAN} + W_{FZL}$, the sum of the plane wave from the interferometer plus the wavefront aberration of the Fresnel zone lens:

$$W_{INT} = W_O + W_R = W_{PLAN} + W_{FZL} = \frac{1}{4}\left(W_1 + W_2 - \overline{W_1} - \overline{W_2}\right) + \frac{1}{2}\left(W_3 + \overline{W_3}\right), \quad (5)$$

where the bar indicates a rotation of the wavefront by 180°.

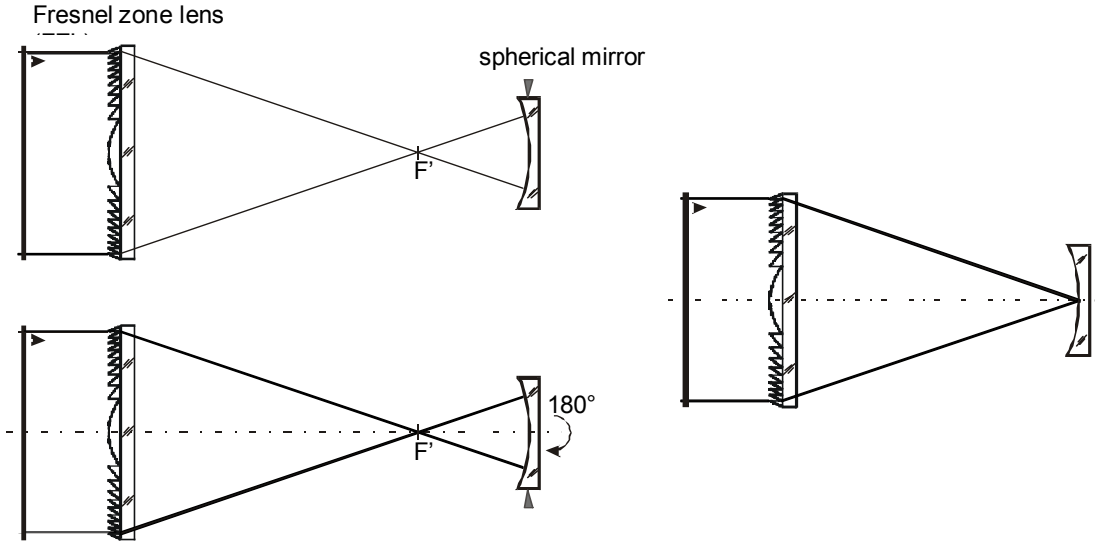

Fig. 3. Required measurements for absolute calibration of the systematic interferometer error W_{INT}

The interferometric test of the diffractive objective was performed with a Twyman-Green interferometer (Fisba µPhase® DCI2) by using phase shifting interferometry. The light source was a He-Ne laser operating at a wavelength of 632.8 nm. Firstly, the three-position test after Jensen was performed with a spherical mirror (Fig. 4). Alignment error terms - defocus and primary coma - were removed from measured data. The aberrations of the spherical mirror W_S and of the plane output wave W_{PLAN} are still included in this synthetic fringe image (see Eq. 4). As a result of this test, the interferometer error $W_{INT} = W_{PLAN} + W_{FZL}$ was estimated absolutely.

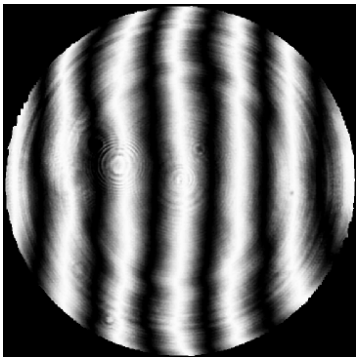

Fig. 4. Synthetic interferogram of the first measurement W_1

However, the plane output wave of the interferometer is also not perfect. The error W_{PLAN} was measured separately with a flat calibration mirror whose accuracy is specified better than λ/10. In Fig. 5(a) the residual wavefront aberration W_{FZL} is shown. To eliminate the influence of alignment errors, Zernike terms tilt, defocus and primary coma were removed from the measured wavefront. The observed PV error of the residual wavefront aberration is 326 nm, the RMS error is 38 nm. Fig. 5(b) visualizes the result of a 10th order Zernike fit [1].

Different error types of the Fresnel zone lens can occur from the fabrication process. There are writing errors of the hologram pattern, depth variations and profile shape errors of the diffractive structure. The first and the second error types result in phase errors of the reconstructed wavefront, if they do not occur only locally. The latter leads to losses in diffraction efficiency of the desired diffraction order. Small local errors, e.g. caused by particles of dust and surface roughness, result in scattered light only.

Wavefront aberrations introduced by the zone plate must be calibrated. The wavefront errors of the zone plate can be separated into figure errors of the CGH substrate, errors of the hologram pattern and depth variations of the diffractive structure. From all error sources, the most important is due to writer distortion. The wavefront error W_{PD} introduced by an incorrect hologram pattern is given by eq. (3).

A detailed discussion of the pattern distortion error and their sources for a circular laser writing system is given in the references [1]. The pattern distortion errors for a circular writing system can be separated in rotationally symmetric and non-rotationally symmetric parts. There is an unique characteristic of a circular writing system, which can be used for estimation and/or characterization of the pattern errors: rotationally symmetric ζ_{RS} and non-rotationally symmetric error parts ζ_{NRS} are independent from each other, caused by different error sources. While a rotationally symmetric writing error is introduced by radial drifts of the writing head relating to the rotation center of the CGH substrate, whereas a non-rotationally symmetric error is caused by runout of the air bearing spindle. So, the radial drift error is constant over the whole azimuth ($\zeta_{RS}(q)$ = const.) and the spindle runout error is identical at a certain angle over the entire radial range ($\zeta_{NRS}(r)$=const.). This allows estimating both error types by a one-dimensional

measurement (e.g. radial drift monitoring during writing process or rotation trajectory measurement by radial/angular scanning of one central circular marker after the hologram writing [7]). The results are combined, and a two-dimensional error estimate is calculated. Methods to specify the writing error and to define the wavefront error function W_{PD} from fabrication data of a specific CGH are described in the references [7].

Here we used an adapted fit procedure to eliminate the *non-rotationally symmetric wavefront error* (spokes error) numerically. In Fig. 5(a) this typical error is clearly visible. The wavefront was weighted by the gradient of the phase function and then fitted by an appropriate polynomial. The result of the numerical elimination procedure is shown in Fig. 6.

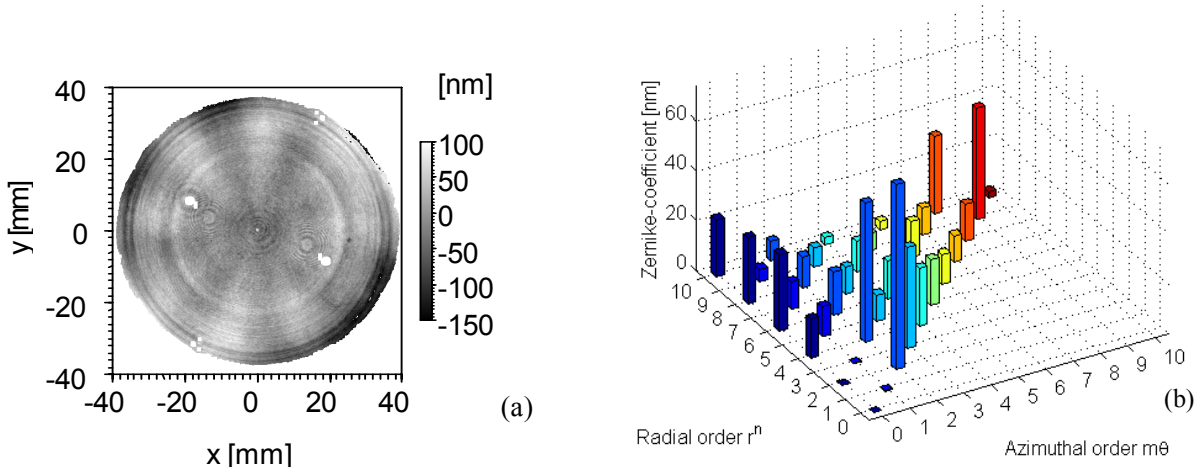

Fig. 5. Residual aberrations of the zone plate $W_{FZL} = W_{INT} - W_{PLAN}$. (a) Wavefront error in double pass with PV=326 nm and RMS = 38 nm. (b) Visualization of a 10th order Zernike fit. Main part of aberrations is astigmatism with A_{22} = 74 nm

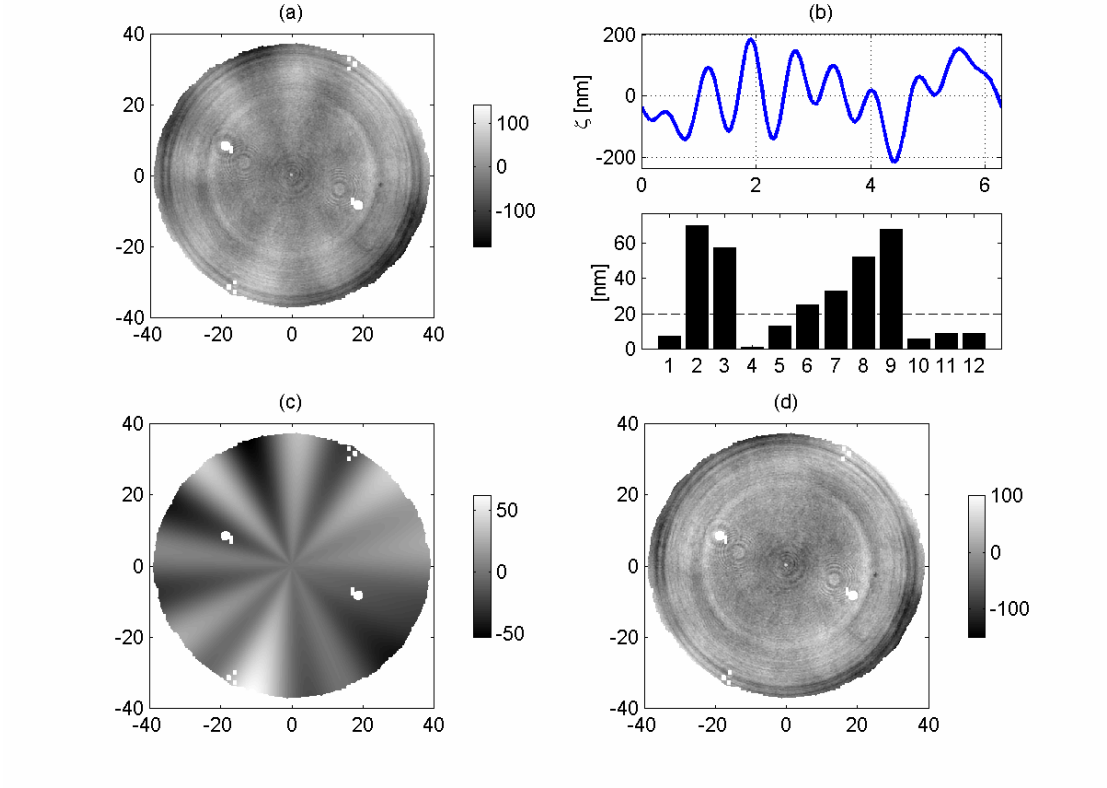

Fig. 6. Numerical elimination of the non-rotationally symmetric wavefront error: (a) Measured wavefront error W_{FZL}, (b) Frequency analysis of the pattern distortion error $\zeta_{PD\,NRS}(\theta)$, (c) Approximation of the non-rotationally symmetric wavefront error, (d) Residual wavefront aberrations after numerical elimination procedure (a) - (c)

The *rotationally symmetric wavefront error* was monitored during the writing process (p.1.1) of the CGH. We used a new monitoring algorithm that measures and saves the position of the markers relative to their known position in the original coordinate system. During the hologram writing the system measures the radial position of the known markers. When the permitted tolerance is locally exceeded the controlling program recalibrates its radial coordinate. To specify the wavefront quality reconstructed by the CGH we used the result of this marker search. The error of the radial coordinate of the current marker gives the current rotationally symmetric pattern distortion error ζ_{RS}. Thus, all quantities from the right side of Eq. (1) are known and therefore, the expected wavefront error due to an incorrect hologram pattern can be evaluated.

In Fig. 7 the expected rotationally symmetric wavefront error is compared with the rotationally symmetric part of the measured wavefront. The rotationally symmetric part of the wavefront was determined by means of the average radial profile of the measured data [1]. Due to this averaging a low-pass filtering occurs and strong phase jumps are smeared. Nevertheless, a good agreement between error prediction and measured error was found, especially for the phase jumps at h = 22 mm and about h = 35 mm.

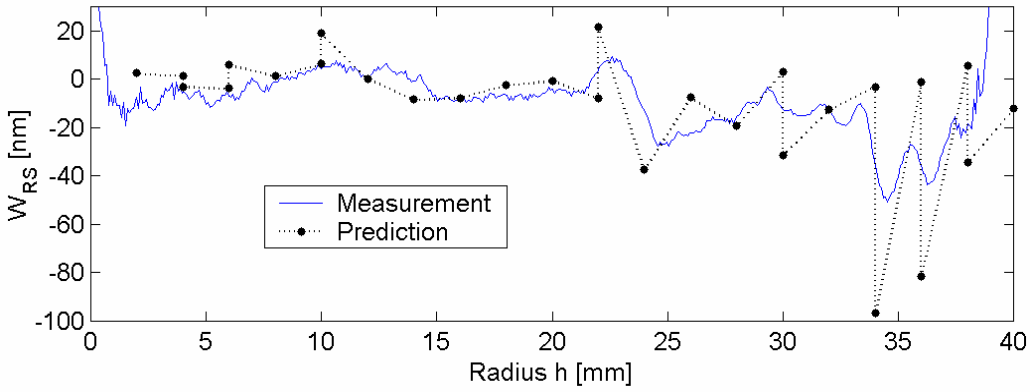

Fig. 7. Comparison between the measured wavefront errors (average radial profile of Fig. 5(a)) and the wavefront error prediction, which was evaluated from the marker search data monitored during the fabrication process and from the design data of the CGH

2.2. Diffraction efficiency

The diffraction efficiency was measured with a small probe beam that probes different areas of the DOE. We measured the efficiency of the DOE only, i.e. the efficiency is the ratio of the intensity in the desired order and the transmitted intensity of an unstructured area of the element. The dependence of diffraction efficiency of a fabricated element over its radius is shown on fig. 8 (a). It is visible that diffraction efficiency reaches 80 % near 5 mm radius (scanning method doesn't allow measuring at low diffraction angles near DOE center) and falls up to 40 % at the periphery of the DOE where zone width was about 4 μm. Total diffraction efficiency of the lens was about 74 %. The drop of diffraction was caused by rounding profile shape near zone boundaries (Fig. 9 (b)). The efficiency can be increased by two methods: fabrication of DOE for second diffraction order or optimization of exposure data with purpose to get sharper sidewalls [12].

Conclusions

We have shown that high precision diffractive objectives can be real alternative to their refractive counterparts. A single-sided prototype has been fabricated by direct laser writing in photoresist. It is well suited for null tests. It can be aligned easily and precisely in the collimated beam of the interferometric setup with the help of the unstructured regions surrounding the actual element.

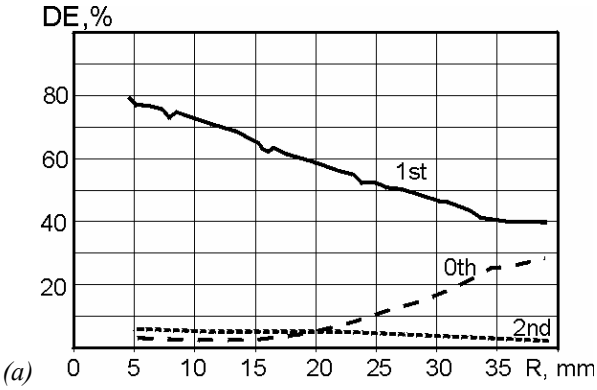

(a)

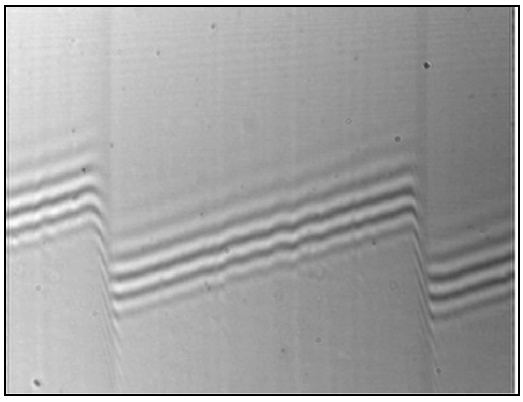

(b)

Fig. 8. (a) Diffraction efficiency of a fabricated element over the radius. (b) Microinterferogram of a diffractive zone with 60 μm width

The element was written on a polar coordinate laser direct writing system that is capable of writing DOEs up to a diameter of 300 mm. The blazed diffractive structures were written directly into a photoresist layer that was spinned on a high-precision substrate. Recalibration of radial coordinate by reading marker position on the substrate was used to eliminate machine drifts. The writing parameters were optimized with the help of modelling the fabrication process in order to maximize the diffraction efficiency. The fabricated objective has a rms wavefront error of less than λ/20 in single pass. The residual errors are predictable on the basis of manufacturing data that is recorded for each element. This allows supplying calibration data for each element. Measurements of the fabricated DOEs show excellent agreement between the predicted and measured wavefront quality.

References

1. N. Buynov, N.P. Larionov, A.V. Lukin, K.S. Mustafin, and R. A. Rafikov Holographic interferometric inspection of aspherical surfaces // *Optical Technology,* 1971. V. **38**. P.194-197.
2. H.J. Tiziani. *Prospects of testing aspheric surfaces with computer generated holograms* // Proc. SPIE, 1981. V. 235. P. 72-79,
3. B. Dörband, H.J. Tiziani. *Testing aspheric surfaces with computergenerated holograms: analysis of adjusment and shape error s*// Applied Optics, 1985. V. 24, No. 16. P. 2604-2611,
4. H.J. Tiziani, B. Packroß, G. Schmidt *Testing of aspheric surfaces with computer generated holograms* // Proceedings of the "International Congress for Ultraprecision Technology", Eds.: M. Weck, R. Hartel, Springer Verlag Berlin, 1988. P. 335-342,
5. V.P. Korolkov, A.I. Malyshev, A.G. Poleshchuk, V.V. Cherkashin, H.J. Tiziani, C. Pruß, T. Schoder, J. Westhauser, C. Wu. *Fabrication of gray-scale masks and diffractive optical elements with LDW-glass //* Proc. SPIE, 2001. V. 4440. P. 73-84.
6. A.G. Poleshchuk, E.G. Churin, V.P. Koronkevich, V.P. Korolkov, A.A. Kharissov, V.V. Cherkashin, V.P. Kiryanov, A.V. Kiryanov, S.A. Kokarev, A.G. Verhoglyad. *Polar coordinate laser pattern generator for fabrication of diffractive optical elements with arbitrary structure //* Applied Optics, 1999. V. **38**, 8. P. 1295-1301.
7. A.G. Poleshchuk, V.P. Korolkov, V.V. Cherkashin, S. Reichelt, J.H. Burge. *Polar coordinate laser writing systems: error analysis of fabricated DOEs //* Proc. SPIE, 2001. V. 4440. P. 161-172,
8. A. E. Jensen. *Absolute calibration method for laser twyman-Green wave-front testing interferometers* // JOSA, 1973. **63,** 1, P. 1313.
9. C.J. Evans, R.E. Parks, P.J. Sullivan, and J.S. Taylor. *Visualization of surface figure by the use of Zernike polynomials* // Applied Optics, 1995. V. **34**. P. 7815-7819,
10. S. Reichelt, M. Daffner, H.J. Tiziani, R. Freimann. *Wavefront aberrations of rotationally symmetric CGHs fabricated by a polar coordinate laser plotter* // accepted for publication in the Journal of Modern Optics, February, 2002.
11. B. Dörband *Evaluation of rotational symmetric surface deviations by means of average radial profile//* Proc. SPIE, 1999. V. 3739. P.474-9,
12. T. Hesller, M.Rossi, R.E. Kunz, M.T. Gale *Analysis and optimization of fabrication of continuous-relief diffrative optical elements* // Applied Optics, 1998. V. **37**. P. 4069-4079.